別紙２

書籍　(2008年度)

著者氏名	連名著者氏名	編集者名	論文タイトル名	書籍名	出版社名	出版地	出版年	開始頁	終了頁
武田元博	小林芳男、小林正樹、桜井　遊、甘利正和、石田孝宣、鈴木昭彦、大内憲明	宇理須恒雄	機能性ナノ粒子による生体イメージング―がん診療への応用―	ナノメディシン ナノテクノ医療応用	オーム社	東京	2008	64	74
樋口秀男	大内憲明	宇理須恒雄	単一量子ドットのバイオ・医療ナノイメージング	ナノメディシン ナノテクノ医療応用	オーム社	東京	2008	52	63
武田元博	権田幸祐、大内憲明	川口春馬	機能性ナノ粒子の医学領域における展開	有機分散系の分散・凝集技術	シーエムシー出版	東京	2008	252	261
大原　智	梅津光央，名嘉　節，高見誠一，阿尻雅文	佐古 猛	超臨界水を用いたナノ粒子製造	超臨界流体技術の開発と応用	シーエムシー出版	東京	2008	56	61

別紙３

学会発表　（2008年度）

国内

第55回日本臨床検査医学会　学術集会、シンポジウム10：医学領域におけるナノ粒子展開をめぐる話題「機能性ナノ粒子による生体イメージングの臨床検査への応用」　2008年11月27－30日、
武田元博、権田幸祐、桜井 遊、河合賢朗、石田孝宣、大内憲明
機能性ナノ粒子による生体イメージングの臨床検査・外科への応用

2008年（平成20年）春季応用物理学関係連合講演会　ナノテクの難病研究・医療への応用、2008年3月27－30日、千葉
武田元博、樋口秀男、小林正樹、小林芳男、大内憲明
機能性ナノ粒子によるナノからマクロレベルの生体イメージング

第31回日本分子生物学会・第81回日本生化学会合同大会、神戸、2008年12月
権田幸祐，渡邉朋信，武田元博，樋口秀男，大内憲明
In vivoイメージングで観えてきた癌転移の仕組み

2009年生体運動合同班会議、東京大学、2009/01/09-10
権田幸祐、渡邉朋信、武田元博、大内憲明、樋口秀男
がん細胞の膜のダイナミックスは転移の進行にともない劇的に変化する

化学工学会第73年会 平成20年3月17－19日、浜松
湊真理絵、小林芳男、武田元博、粕谷厚生、大内憲明
AgI/SiO2複合粒子コロイドの調製法の開発

第１８回乳癌基礎研究会、平成20年7月12-13日、福島
河合賢朗、武田元博、石田孝宣、大内憲明
粒径の異なるナノ粒子による腫瘍間質ドラッグデリバリーシステムの解析

第125回バイオメカニクス研究会（日本生体医工学会専門別研究会）、（東北大）2008年 10月
権田幸祐、武田元博、樋口秀男、大内憲明
In vivoナノイメージングで観えてきた癌転移の仕組み

ナノ学会第６回大会、福岡、2008/05/07-09
権田幸祐，渡邉朋信，武田元博，大内憲明，樋口秀男
量子ドットを用いた腫瘍細胞の膜伸縮運動のin vivoイメージング

ナノ学会第６回大会、福岡、2008/05/07-09
叢莉蔓、小林芳男、武田元博、櫻井遊、甘利正和、大内憲明
シリカコーティング蛍光ナノビーズによるセンチネルリンパ節生検と分子画像診断

ナノ学会第６回大会、福岡、2008/05/07-09
武田元博、小林芳男、小林正樹、桜井遊、権田幸祐、樋口秀男、大内憲明
ナノヨウ化銀ビーズによるCT造影法の外科応用に関する基礎的検討

ナノ学会第６回大会、福岡、2008/05/07-09（若手優秀発表賞受賞）
河合賢朗、武田元博、石田孝宣、大内憲明
蛍光ナノ粒子を用いた担がんマウスにおける腫瘍間質ナノドラッグデリバリーシステムの解析

ナノ学会第６回大会、福岡、2008/05/07-09
日景充、亀井尚、武田元博、小林正樹、大内憲明
新規ナノ粒子をトレーサーとした鏡視下手術の基礎的検討

第108回日本外科学会定期学術集会、長崎、2008/05/15-17
河合賢朗、樋口秀男、武田元博、石田孝宣、鈴木昭彦、甘利正和、宇佐美伸、桜井遊、渡部剛、
腫瘍間質におけるナノスケールでの分子挙動解析によるDDSの解明

異分野融合ナノテクノロジー横浜コロキウム、平成20年2月1日、横浜
武田元博、樋口秀男、大内憲明
機能性ナノ粒子の医学領域における展開

第１８回乳癌基礎研究会、平成20年7月12-13日、福島
武田元博、河野雅弘、佐藤恵美子、山田理恵、甘利正和、鈴木昭彦、石田孝宣、大内憲明
ヘマトポルフィリン誘導体計測によるがん診断の基礎的検討

平成20年年度電気関係学会東北支部連合大会，講演番号2E14，講演論文集p. 183（2008）
南部雄也，鈴木知佳，高橋誠樹，Trinh Quang Duc，小林正樹
超音波タグ蛍光断層イメージング法による生体組織の蛍光断層画像計測

平成20年年度電気関係学会東北支部連合大会，講演番号2E15，講演論文集p. 184（2008）
熊坂増高，日景允，亀井尚，武田元博，大内憲明，小林正樹
ナノ蛍光微粒子によるセンチネルリンパ節検索のための腹腔内視鏡蛍光イメージングシステムの

第６０回日本細胞生物学会　ワークショップ（パシフィコ横浜）2008年 7月
権田幸祐，渡邉朋信，武田元博，大内憲明，樋口秀男
量子ドットを用いた腫瘍細胞のin vivoイメージング

第61回コロイドおよび界面化学討論会平成20年9月
湊真理絵、小林芳男、武田元博、粕谷厚生、大内憲明
医療検査用コア - シェル型複合粒子の合成に関する研究

国際（海外）

Ohuchi N, Takeda M, Kawai M, Tada H, Sakurai Y, Gonda K, Higuchi H.
Novel imaging techniques with functional nano-objects for cancer diagnosis
Hot Topics in Molecular Imaging 2008 (TOPIM'08), Eiropean Society for Molecular Imaging, Les Houches, France, February 4-8, 2008.

Kawai M, Higuchi H, Gonda K, Takeda M, Ohuchi N.
In vivo imaging of vascular permeability using nano-objects in mice tumor.
Hot Topics in Molecular Imaging 2008 (TOPIM'08), Eiropean Society for Molecular Imaging, Les Houches, France, February 4-8, 2008.

Ohuchi N, Takeda M, Kawai M, Tada H, Sakurai Y, Gonda K, Higuchi H.
Molecular imaging with functional nano-objects for cancer diagnosis.
The 5th International Symposium on Nano-Biomedical Engineering Education and Research Centre. March, 27-28, 2008, Matsushima, Japan

Ishida T, Kiba T, Takeda M, Matsuyama K, Teramukai S, Masuda N, Takatsuka Y, Noguchi S, Fukushima M, Ohuchi N.
Phase II study of Capecitabine and Trastuzumab combination chemotherapy in patients with HER2 overexpressing metastatic breast cancers after failure of both Anthracyclines and Taxanes.
The 44th American Society of Clinical Oncology (ASCO) Annual Meeting, May 30 - June 3, 2008,

Suzuki T, Moriya T, Hayashi S, Ohuchi N, Sasano H.
Intratumoral concentration of sex stereoids in ductal carcinoma in situ (DCIS) of human breast. Breast Cancer, 15, Supplement 1, 10-10, 2008
The 26th Congress of the International Association for Breast Cancer Research, September 22-24, 2008, Kurashiki, Japan

Nakano T, Tse GM, Tan PH, Kozuka Y, Kanomata N, Ishida T, Ishida K, Watanabe M, Tamaki K, Ohuchi N, Sasano H, Moriya T.
Triple negative subtype of ductal carcinoma in situ in Asian women. Breast Cancer, 15, Supplement 1,
The 26th Congress of the International Association for Breast Cancer Research, September 22-24, 2008, Kurashiki, Japan

Kozuka Y, Moriya T, Akiyama F, Kurosumi M, Tse GM, Tan PH, Kanomata N, Ohuchi N, Kurebayashi J,
Breast Cancer, 15, Supplement 1, 19-20, 2008
The 26th Congress of the International Association for Breast Cancer Research, September 22-24, 2008, Kurashiki, Japan

Kawai M, Takeda m, Ishida T, Suzuki A, amari M, Ohuchi N.
Breast Cancer, 15, Supplement 1, 33-33, 2008
The 26th Congress of the International Association for Breast Cancer Research, September 22-24, 2008, Kurashiki, Japan

Takeda M, Sakurai Y, Kobayashi Y, Cong L, Hikage M, Amari M, Ishida T, Gonda K, Ohuchi N.
Breast Cancer, 15, Supplement 1, 37-37, 2008
The 26th Congress of the International Association for Breast Cancer Research, September 22-24, 2008, Kurashiki, Japan

Harada N, Yamada T, Ishida T, Takeda Suzuki A, Amari M, Moriya T, Ohuchi N.
Breast Cancer, 15, Supplement 1, 36-36, 2008
The 26th Congress of the International Association for Breast Cancer Research, September 22-24, 2008, Kurashiki, Japan

Noriaki Ohuchi
Plenary lecture: Drug resistance as a target for cancer chemotherapy by Fujita N
The 26th Congress of the International Association for Breast Cancer Research, September 22-24, 2008, Kurashiki, Japan (Chairman)

Gonda, K., Takeda, M., Kawai, M., Sakurai Y, Higuchi H., Ohuchi, N.
Imaging of cancer metastasis in living tumor with quantum dots.
The 7th International Symposium on Nano-Biomedical Engineering, October 2008, National Cheng Kung University, Tainan

Takeda M, Tada H, Kawai, M, Sakurai Y, Cong L, Gonda K, Higuchi H, Ohuchi N.
Bio-imaging by functional nano-particles of nano to macro scale.
The 13th Internatonal Conferencenon Biomedical Engineering, December 3-6.2008, Singapore

Kawai, M, Takeda M, Ohuchi N.
The feature of the interstitial nano drug delivery system with fluorescent nanocrystals of different sizes in the human tumor xenograft in mice.
The 13th Internatonal Conferencenon Biomedical Engineering, December 3-6.2008, Singapore

Cong L, Takeda M, Watanabe M, Kobayashi Y, Kobayashi M, Ohuchi N.
Silica-coated fuorescent nano-Particles for sentinel lymph node biopsy and mapping.
Tohoku-NUS student joint symposium. December 9-10, 2008, Singapore.

Gonda K, Watanabe TM, Takeda M, Higuchi H and Ohuchi N.
In vivo imaging of membrane dynamics in metastatic tumor cells.
The 2nd International Symposium on Nanomedicine, Asian Core Symposium-Nano and Biomedical Molecular Science-, February 4-7, 2009, Okazaki, Japan.

Q. D. Trinh, Y. Nanbu, T. Suzuki, S. Takahashi, M. Takeda, M. Kobayashi M.
Basic study on application of the phased-array transducer to determine fluorescence in turbid media based-on acousto-optic effects.
International Conference on Laser Applications in Life Sciences (LALS 2008), Abstract book p. 7 (Taipei, Taiwan) (December 4 2008)

Q. D. Trinh, Y. Nanbu, T. Suzuki, S. Takahashi, M. Takeda, M. Kobayashi M.
Fluorescence tomography based-on acousto-optic modulations with phased-array ultrasound transducer.
BiOS Part of SPIE Photonic West, paper No. 7177-57 (San Jose, USA) (January 27, 2009)

別紙4

特許財産権の出願登録状況　(2008年)

内容	発明者	権利者	知的財産権の種類	番号	出願年月日	取得年月日
がん細胞運動およびがん細胞浸潤抑制剤	権田幸祐、樋口秀	東北大学	特許出願	特願2008－083588	2008. 3. 27	

Ⅳ. 研究成果の刊行物・別刷

Preparation of amine free silica-coated AgI nanoparticles with modified Stöber method

Y. Kobayashi[1,2]*, N. Shimizu[1], K. Misawa[1], M. Takeda[3], N. Ohuchi[3], A. Kasuya[4] and M. Konno[1]

In recent years, the authors studied on fabrication of silica-coated AgI (AgI–SiO_2) nanoparticles with a Stöber method toward new X-ray contrast agents. In the Stöber method, amines are often used as catalysts for silica formation, so that it is probable that amine is left in the silica-coated particles. Since amines are harmful to the human body, amine free particles are desired for medical use. From this viewpoint, amine free AgI–SiO_2 nanoparticles were prepared with a modified Stöber method using NaOH as a catalyst instead of amine in the present work. The AgI nanoparticles were prepared from $AgClO_4$ and KI with the use of 3-mercaptopropyltrimethoxysilane (MPS) as a silane coupling agent and NaOH catalyst for alkoxide hydrolysis. The silica-coating was performed at $4{\cdot}5 \times 10^{-5}$M MPS, 15–22·5M water, 0·0008–0·0024M NaOH and 0·0004–0·009M tetraethylorthosilicate at an AgI concentration of 0·001M. AgI–SiO_2 particles as small as ca. 30 nm could be successfully fabricated at the concentrations of $4{\cdot}5 \times 10^{-5}$M MPS, 20M water, 0·0011M NaOH, 0·001M AgI and 0·004M tetraethylorthosilicate.

Keywords: AgI, Nanoparticle, Core–shell, Silica coating, Sol–gel, Stöber method

Introduction

Iodine compounds have been used as X-ray contrast agents in the field of medicine,[1] because of their low transmittance property for X-ray. The iodine compounds may provoke adverse events as allergic reactions in patients,[1] so that they cannot be administered to such people. Core–shell nanoparticles are good candidates for prevention of allergic reactions, because the shell materials can keep the contrast agents from living systems.

Silica coating of metal naoparticles has been intensively studied by Liz-Marzán *et al.*[2] Giersig *et al.* extended the silica-coating technique to fabrication of silica coated AgI nanoparticles, which employed a reaction of silica-coated Ag nanoparticles with I_2 for formation of AgI.[3]

The authors proposed an alternative method for silica-coating of an iodine compound AgI with a Stöber method,[4–6] and obtained silica coated AgI nanoparticles contrast agents for X-ray computed tomography.[7] However, in the Stöber method, amines are often used as catalysts for silica formation,[8] so that it is probable that amine is left in the silica-coated particles. Since amines are harmful to the human body,[9,10] amine free particles are desired for medical use. For producing amine free silica-coated AgI nanoparticles, the present work proposes a modified method using NaOH as the catalyst instead of amine.

[1]Department of Chemical Engineering, Graduate School of Engineering, Tohoku University, Aoba, Aramaki-aza, Aoba-ku, Sendai 980-8579, Japan
[2]Department of Biomolecular Functional Engineering, Faculty of Engineering, Ibaraki University, 4-12-1 Nakanarusawa-cho, Hitachi, Ibaraki 316-8511, Japan
[3]Division of Surgical Oncology, Graduate School of Medicine, Tohoku University, Seiryo-machi, Aoba-ku, Sendai 980-8574, Japan
[4]Centre for Interdisciplinary Research, Tohoku University, Aoba, Aramakiaza, Aobaku, Sendai 980-8578, Japan

*Corresponding author, email ykoba@mx.ibaraki.ac.jp

Experimental

Chemicals

$AgClO_4$ (Kanto Chemical Co., Inc., 99%) and KI (Wako Pure Chemicals Ltd, 99·5%) were used as AgI precursors. Tetraethylorthosilicate (TEOS) (Wako Pure Chemicals Ltd, 95%), 3-mercaptopropyltrimethoxysilane (MPS) (Aldrich, 97%) and ethanol (Wako Pure Chemicals Ltd, 99·5%) were used for silica coating, and sodium hydroxide (NaOH) (Wako Pure Chemicals Ltd, 0·1M) was used as a catalyst for a sol–gel reaction of TEOS and MPS. All chemicals were used as received. Ultrapure deionised water (resistivity higher than 18 MΩ cm) was used in all the preparations.

Preparation of materials

Colloids of AgI nanoparticles were prepared by mixing of $AgClO_4$ and KI solutions at a constant Ag/I molar ratio of 1 : 2, as follows. A freshly prepared 2M $AgClO_4$ aqueous solution (0·015 mL) was added to 0·05M KI aqueous solution (6 mL) under vigorous stirring at room temperature to provide an AgI concentration of 5×10^{-3}M. Immediately after the mixing, colour of the solution turned yellow. The Stöber method with TEOS was applied to silica-coating of the AgI nanoparticles. To the AgI colloid was added an aqueous MPS solution. After 15 min, ethanol and TEOS were successively

Published by Maney on behalf of the Institute
Received 21 December 2007; accepted 14 March 2008
DOI 10.1179/174329408X315409

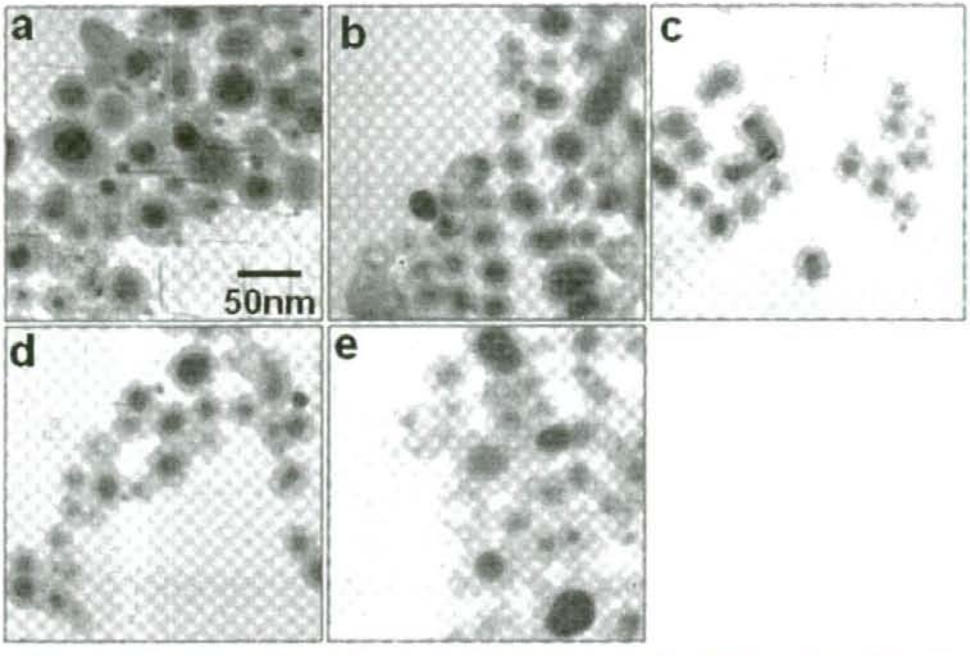

1 Images (TEM) of AgI–SiO_2 particles prepared at NaOH concentrations of *a* 0·0008, *b* 0·0009, *c* 0·001, *d* 0·0011 and *e* 0·0012M: initial concentrations of $AgClO_4$, KI, MPS, H_2O and TEOS were $1·0\times10^{-3}$, $2·0\times10^{-3}$, $4·5\times10^{-5}$, 20 and 0·004M with respect to total solution volume

added to the colloid. Then, the silica-coating was initiated by rapidly injecting an aqueous NaOH solution into the AgI/TEOS colloid. Initial concentrations of NaOH, H_2O and TEOS were varied from 0·0008 to 0·0024M, from 15 to 22·5M and from 0·0004 to 0·009M respectively, while initial concentrations of $AgClO_4$, KI and MPS were 0·001, 0·002 and $4·5\times10^{-5}$M respectively.

Characterisation

The AgI–SiO_2 particles were characterised by transmission electron microscopy (TEM) with a Zeiss LEO 912 OMEGA operating at 100 kV. Samples for TEM were prepared by dropping and evaporating the nanoparticle suspensions on a collodion coated copper grid. Silica shell thickness was estimated as the difference between AgI particle and composite particle sizes. Ultraviolet-visible (UV-VIS) extinction spectra were measured with a Hitachi UV-3010 spectrophotometer. X-ray diffraction (XRD) measurements were made with a Rigaku RU-200A diffractometer at 40 kV and 30 mA with Cu K_γ radiation.

Results and discussion

Effect of NaOH concentration

Figure 1 shows the TEM images of AgI–SiO_2 particles prepared at various NaOH concentrations. At concentrations of 0·0008 and 0·0009M, shell free AgI nanoparticles were obtained due to a shortage of NaOH catalyst, though some silica coated AgI particles were also prepared. At 0·0010 and 0·0011M, the AgI nanoparticles were well coated with silica. Addition of NaOH probably increased the ionic strength of the solution. Thus, the increased ionic strength should reduce the double layer repulsion between the AgI nanoparticles and the silica nuclei. As a result, the silica nuclei were efficiently deposited on the AgI particle surfaces. When an NaOH concentration increased to 0·0012M, AgI cores in the AgI–SiO_2 particles became large. The further increased ionic strength would promote both aggregation and growth of AgI cores before silica coating. Besides, aggregation of the AgI–SiO_2 particles was observed. The increased ionic strength also provided the particle aggregation after silica-coating.

Effect of H_2O concentration

Figure 2 shows the TEM images of AgI–SiO_2 particles prepared at various H_2O concentrations. At concentrations of 20 and 22·5M, quasi-perfect core–shell structure was formed. Core–shell particles were also produced for concentrations as low as 15 and 17·5M. Compared to the high H_2O concentrations, the AgI cores were large. Because the dielectric constant of water/ethanol solution is low at low H_2O concentration, silanol groups on the surface of MPS modified AgI particles probably tend to deionise in the water/ethanol solution. Thus, the electrostatic repulsion between the AgI particles was weak, and thereby the AgI nanoparticles aggregated and grew in the water/ethanol solution before silica-coating. In addition, coalescence of the AgI–SiO_2 particles was observed. The low dielectric constant also provided deionisation of silanol groups on the surface of

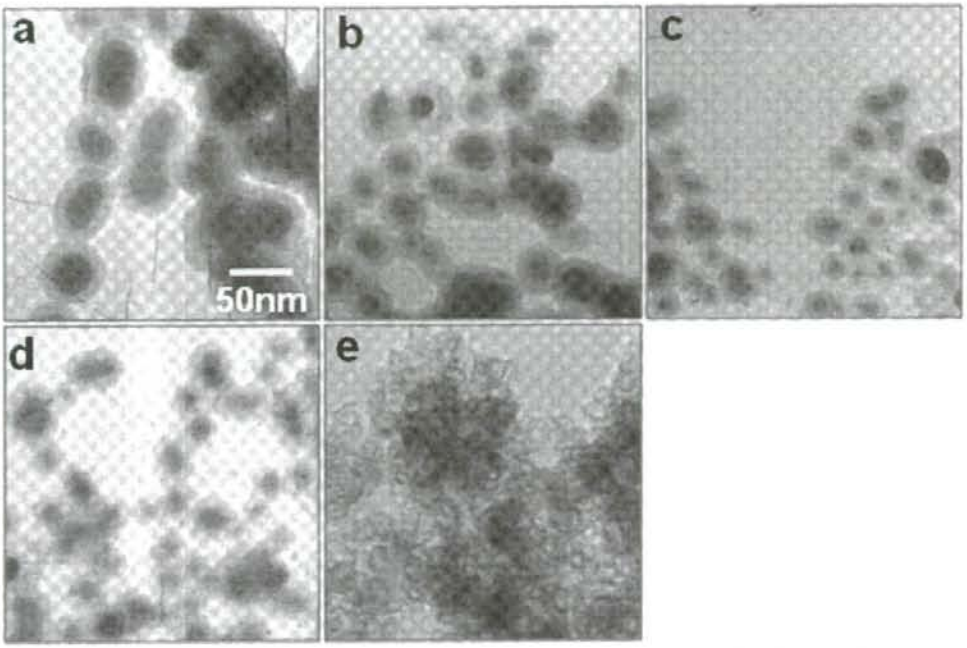

2 Images (TEM) of AgI–SiO_2 particles prepared at H_2O concentrations of *a* 15, *b* 17·5, *c* 20, *d* 22·5 and *e* 25M: initial concentrations of $AgClO_4$, KI, MPS, NaOH and TEOS were $1{\cdot}0\times10^{-3}$, $2{\cdot}0\times10^{-3}$, $4{\cdot}5\times10^{-5}$, 0·0011 and 0·004M with respect to total solution volume

AgI–SiO_2 particles. Consequently, the coalescence took place with a similar mechanism to the formation of large AgI cores. For a concentration as high as 25M, many secondary silica particles were produced. In contrary to the low H_2O concentration, the high H_2O concentration probably provides ionisation of silanol groups on the silica particle surface. Thus, the electrostatic repulsion between generated particles also increased. Therefore, silica nuclei generated during the early stages of the sol–gel reaction probably grew as stable secondary silica particles rather than on the existing cores.

Effect of TEOS concentration

Figure 3 shows the TEM images of AgI–SiO_2 particles prepared at various TEOS concentrations. At the concentrations of 0·0004 and 0·001M (Figs. 3*a* and *b*), no core–shell structure was formed, though a few core–shell particles were also produced for 0·001M. This result indicated that the amount of TEOS was not enough to coat AgI nanoparticles. For 0·004–0·009M (Figs. 3*c–f*), most of the particles were quasi-perfect core–shells with just one AgI core with a size ~20 nm. An average size of the AgI–SiO_2 particles was varied from 28·3 to 32·2 nm with the increase in TEOS concentration from 0·004 to 0·009M.

Ultraviolet-visible spectroscopy

Figure 4 gives the absorption spectrum of AgI–SiO_2 particle colloid. A sharp peak ~421 nm and a shoulder peak ~330 nm were observed, which were attributed to exciton peaks of AgI.[11–14] Thus, the existence of AgI nanoparticles was confirmed from the UV-VIS spectroscopy.

X-ray diffraction

Figure 5 shows the XRD pattern of AgI–SiO_2 particles. Peaks were observed at 22·4, 23·7, 25·4, 32·8, 39·2, 42·7 and 46·4°. Although these peaks were all attributable to β-AgI,[14] all peaks of γ-AgI overlap with the peaks of 002 (23·7°), 110 (39·2°) and 112 (46·4°) of β-AgI. Accordingly, the XRD measurement revealed that the obtained AgI nanoparticles were β-AgI or a mixture of β-AgI and γ-AgI.

Conclusion

AgI–SiO_2 particles were prepared by employing a sol–gel reaction of TEOS with NaOH catalyst in the presence of MPS modified AgI nanoparticles for producing AgI–SiO_2 particle colloid. Concentration effects of NaOH, H_2O and TEOS can probably be explained by the differences of the solution in dielectric constant and ionic strength. The coating reaction at $4{\cdot}5\times10^{-5}$M MPS, 20 M H_2O, 0·0011M NaOH, 0·001M AgI and 0·004–0·009M TEOS provided formation of AgI–silica core–shell structure that had sizes of ca. 30 nm.

Acknowledgement

This research was partially supported by the Ministry of Education, Culture, Sports, Science and Technology of

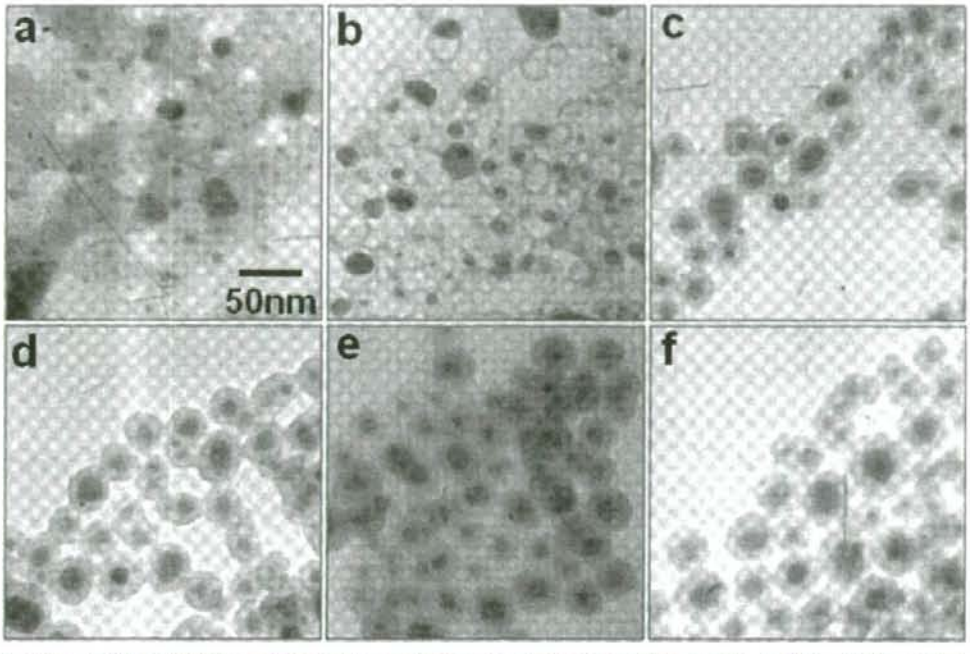

3 Images (TEM) of AgI–SiO_2 particles prepared at TEOS concentrations of *a* 0·0004, *b* 0·001, *c* 0·004, *d* 0·006, *e* 0·008 and *f* 0·009M: initial concentrations of $AgClO_4$, KI, MPS, H_2O and NaOH were $1·0\times10^{-3}$, $2·0\times10^{-3}$, $4·5\times10^{-5}$, 20 and 0·0011M with respect to total solution volume

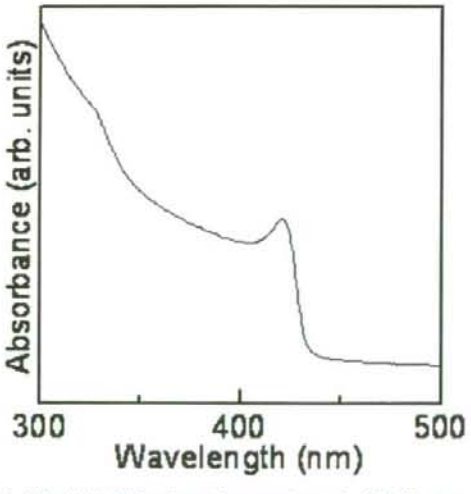

4 Ultraviolet-visible absorption spectrum of AgI–SiO_2 particle colloid: initial concentrations of $AgClO_4$, KI, MPS, H_2O NaOH and TEOS were $1·0\times10^{-3}$, $2·0\times10^{-3}$, $4·5\times10^{-5}$, 20, 0·0011 and 0·008M with respect to total solution volume

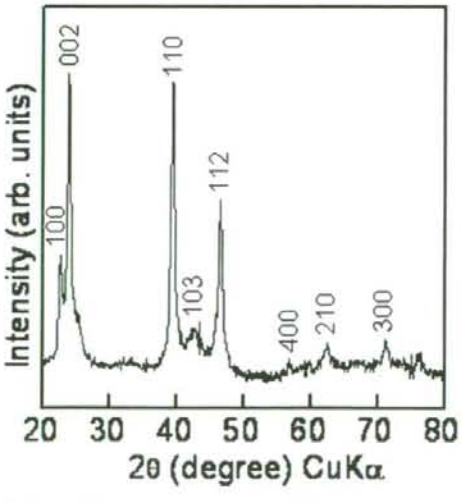

5 X-ray diffraction pattern of AgI–SiO_2 particles: initial concentrations of $AgClO_4$, KI, MPS, H_2O NaOH and TEOS were same as Fig. 4

Japan (Grant-in-Aid for the COE project, Giant Molecules and Complex Systems), and by the Ministry of Health, Labour and Welfare of Japan.

References

1. A. Joubert, M.-C. Biston, C. Boudou, J.-L. Ravanat, T. Brochard, A.-M. Charvet, F. Estève, J. Balosso and N. Foray: *Int. J. Radiat. Oncol. Biol. Phys.*, 2005, **62**, 1486–1496.

2. L. M. Liz-Marzán, M. Giersig and P. Mulvaney: *Langmuir*, 1996, **12**, 4329–4335.
3. M. Giersig, L. M. Liz-Marzán, T. Ung, D. Su and P. Mulvaney: *Ber. Bunsen-Ges. Phys. Chem.*, 1997, **101**, 1617–1620.
4. Y. Kobayashi, K. Misawa, M. Takeda, M. Kobayashi, M. Satake, Y. Kawazoe, N. Ohuchi, A. Kasuya and M. Konno: *Colloids Surf. A*, 2004, **251A**, 197–201.
5. Y. Kobayashi, K. Misawa, M. Takeda, M. Kobayashi, M. Satake, Y. Kawazoe, N. Ohuchi, A. Kasuya and M. Konno: Proc. 12th Int. Conf. Composites/Nano Eng. (ICCE-12) on 'Silica-coating of AgI nanoparticles using a modified Stöber method', Tenerife, Spain, August 2005, University of New Orleans.
6. Y. Kobayashi, K. Misawa, M. Takeda, N. Ohuchi, A. Kasuya and M. Konno: Proc. 4th Int. Conf. Adv. Mater. Process. (ICAMP-4) on 'Control of shell thickness in silica-coating of AgI nanoparticles', Hamilton, New Zealand, December 2006, The University of Waikato, 033.
7. Y. Sakurai, M. Takeda, Y. Kawazoe, A. Kasuya, Y. Kobayashi, T. Kamei, M. Nakajima and N. Ohuchi: *Breast Dis.*, 2006, **25**, 55–56.
8. W. Stöber, A. Fink and E. Bohn: *J. Colloid Interface Sci.*, 1968, **26**, 62–69.
9. S. C. Mitchell and A. Q. Zhang: *Clin. Chim. Acta*, 2001, **312**, 107–114.
10. R. Benigni and L. Passerini: *Mutat. Res.*, 2002, **511**, 191–206.
11. H. Vogelsang, O. Husberg and W. von der Osten: *J. Lumin.*, 2000, **86**, 87–94.
12. S. Kondo, T. Itoh and T. Saito: *Phys. Rev. B*, 1998, **57B**, 13235–13240.
13. P. S. Kumar, P. B. Dayal and C. S. Sunandana: *Thin Solid Films*, 1999, **357**, 111–118.
14. Y. Wang, J. Mo, W. Cai, L. Yao and L. Zhang: *Mater. Lett.*, 2002, **56**, 502–506.

Biomed Microdevices (2008) 10:153–167
DOI 10.1007/s10544-007-9121-z

In vitro blood flow in a rectangular PDMS microchannel: experimental observations using a confocal micro-PIV system

Rui Lima · Shigeo Wada · Shuji Tanaka · Motohiro Takeda · Takuji Ishikawa · Ken-ichi Tsubota · Yohsuke Imai · Takami Yamaguchi

Published online: 18 September 2007

Abstract Progress in microfabricated technologies has attracted the attention of researchers in several areas, including microcirculation. Microfluidic devices are expected to provide powerful tools not only to better understand the biophysical behavior of blood flow in microvessels, but also for disease diagnosis. Such microfluidic devices for biomedical applications must be compatible with state-of-the-art flow measuring techniques, such as confocal microparticle image velocimetry (PIV). This confocal system has the ability to not only quantify flow patterns inside microchannels with high spatial and temporal resolution, but can also be used to obtain velocity measurements for several optically sectioned images along the depth of the microchannel. In this study, we investigated the ability to obtain velocity measurements using physiological saline (PS) and *in vitro* blood in a rectangular polydimethysiloxane (PDMS) microchannel (300 μm wide, 45 μm deep) using a confocal micro-PIV system. Applying this combination, measurements of trace particles seeded in the flow were performed for both fluids at a constant flow rate (Re = 0.02). Velocity profiles were acquired by successive measurements at different depth positions to obtain three-dimensional (3-D) information on the behavior of both fluid flows. Generally, the velocity profiles were found to be markedly blunt in the central region, mainly due to the low aspect ratio (h/w = 0.15) of the rectangular microchannel. Predictions using a theoretical model for the rectangular microchannel corresponded quite well with the experimental micro-PIV results for the PS fluid. However, for the *in vitro*

R. Lima · M. Takeda · T. Ishikawa · K.-i. Tsubota · Y. Imai · T. Yamaguchi
Department of Bioengineering and Robotics,
Graduate School of Engineering, Tohoku University,
6-6-01 Aoba,
980-8579 Sendai, Japan

R. Lima
Department of Mechanical Tech, ESTiG, Braganca Polyt.,
C. Sta. Apolonia,
5301-857 Braganca, Portugal

S. Wada
Department of Mechanical Science and Bioengineering,
Graduate School of Engineering Science, Osaka University,
Toyonaka 560-8531 Osaka, Japan

S. Tanaka
Department of Nanomechanics, Graduate School of Engineering,
Tohoku University,
6-6-01 Aoba,
980-8579 Sendai, Japan

M. Takeda
Division of Surgical Oncology, Graduate School of Medicine,
Tohoku University,
2-1 Seiryo-machi, Aoba-ku,
980-8575 Sendai, Japan

R. Lima (✉)
Yamaguchi and Ishikawa Lab. (PFSL), Department of
Bioengineering and Robotics, Graduate School of Engineering,
Tohoku University,
6-6-01 Aoba,
980-8579 Sendai, Japan
e-mail: rui@pfsl.mech.tohoku.ac.jp

blood with 20% hematocrit, small fluctuations were found in the velocity profiles. The present study clearly shows that confocal micro-PIV can be effectively integrated with a PDMS microchannel and used to obtain blood velocity profiles along the full depth of the microchannel because of its unique 3-D optical sectioning ability. Advantages and disadvantages of PDMS microchannels over glass capillaries are also discussed.

Keywords Microcirculation · Confocal micro-PIV · PDMS microchannel · Red blood cells · Mesoscopic blood flow

1 Introduction

Blood is not a homogeneous fluid, but one composed mainly of a suspension of red blood cells (RBCs) in plasma. In addition, the non-continuum behavior of blood flow through microvessels leads to complex flow mechanics, which are not yet clearly understood (Goldsmith and Turitto 1986; Secomb 1995; Mchedlishvili and Maeda 2001). Because several important physiological and pathological phenomena occur in the microcirculation, velocity profiles have been intensively studied both *in vivo* (Einav et al. 1975; Tangelder et al. 1986; Golster et al. 1999; Parthasarathi et al. 1999; Nakano et al. 2003) and *in vitro* (Gaehtgens et al. 1970; Baker and Wayland 1974; Born et al. 1978; Cochrane et al. 1981; Gaehtgens 1987; Uijttewaal et al. 1994; Alonso et al. 1995; Moger et al. 2004; Kim and Lee 2006; Lima et al. 2007) using several blood flow measuring techniques. Both *in vivo* and *in vitro* experiments have played important roles in our understanding of several phenomena in the microcirculation. Although several comprehensive reviews about blood flow behavior in microvessels have been published (Caro et al. 1978; Chien et al. 1984; Secomb 1995; Mchedlishvili and Maeda 2001; Pries and Secomb 2003), much remains unknown about physiological and pathological phenomena occurring in the microcirculation.

Historically, the most commonly used experimental techniques to study blood flow in the microcirculation have been double-slit photometry (Gaehtgens et al. 1970; Baker and Wayland 1974), video microscopy and image analysis (Bugliarello et al. 1963; Tangelder et al. 1986; Goldsmith and Turitto 1986; Gaehtgens 1987; Alonso et al. 1995; Parthasarathi et al. 1999; Tsukada et al. 2000), and laser-Doppler anemometry (Einav et al. 1975; Born et al. 1978; Cochrane et al. 1981; Uijttewaal et al. 1994; Golster et al. 1999). However, with these techniques, both spatial resolution and velocity accuracy are unsatisfactory.

In recent years, because of advances in computers, optics, and digital image processing techniques, it has become possible to combine a conventional particle image velocimetry (PIV) system (Adrian 1991; Raffel et al. 1998) with an inverted epifluorescent microscope (Santiago et al. 1998; Koutsiaris et al. 1999). As a result, this combination, known as a micro-PIV, has greatly increased the resolution of conventional PIV. Because of the success of micro-PIV in measuring accurate velocity fields of homogeneous fluids in microfluidic devices (Nguyen and Wereley 2002), the technique has been recently used to investigate blood flow behavior in both microchannels and microvessels (Nakano et al. 2003; Bitsch et al. 2005; Vennemann et al. 2006).

Although the conventional PIV technique has proven useful in measuring blood flow velocities in microvessels, the entire flow field is illuminated and consequently the out-of-focus emitted light can result in high levels of background noise, which degrades the measured velocity fields (Meinhart et al. 2000; Nguyen and Wereley 2002). One way to minimize the depth-of-focus effect is using a confocal micro-PIV (Tanaani et al. 2002; Kinoshita et al. 2005; Lima et al. 2005, 2006) or confocal laser scanning microscopy (CLSM) micro-PIV (Park et al. 2004, 2006). This technique combines the conventional PIV system with a spinning disk confocal microscope (SDCM), which has the ability to obtain in-focus images with an optical thickness less than 1 μm (optical sectioning effect). Park et al. (2004, 2006) compared confocal micro-PIV with conventional micro-PIV and demonstrated that the former had improved particle image contrast and definition, allowing more accurate velocity measurements (see Table 1). As a result, by combining SDCM with a conventional PIV system, it is possible to achieve a PIV system with high spatial resolution able to generate velocity profiles at several optically sectioned planes along the microchannel depth.

Progress in microfabricated technologies has attracted the attention of the biomedical research community to the development of diagnostic, microfluidic devices (so-called bio-micro-electromechanical systems or a lab-on-a-chip; Sutton et al. 1997; Gomez et al. 2001; Beebe et al. 2002; Gifford et al. 2003; Minas et al. 2004; Toner and Irimia

Table 1 The lateral and axial resolutions of both conventional and confocal microscopes and optical slice thickness of confocal microscopes (Willhelm et al. 2003; Park et al. 2004)

Optical resolutions	Conventional microscopy		Confocal microscopy (SDCM)	
	40×	10×	40×	10×
Lateral resolution (μm)	0.418	1.047	0.331	0.829
Axial resolution (μm)	1.831	11.444	1.268	9.323
Optical slice thickness (μm)	Not definable		2.820	26.701

2005; Faivre et al. 2006) capable of providing useful information about the general health status of patients. However, most of the information provided by blood analysis in microchannels is based on conventional visual observations on the area and volume of the RBCs (Sutton et al. 1997; Gifford et al. 2003). We believe that the acquisition of quantitative blood flow measurements may also provide relevant information for the diagnosis of disease and the treatment of patients.

Recently, we demonstrated the ability of the confocal micro-PIV to measure both pure water and diluted suspensions of blood cells in a glass square microchannel (Lima et al. 2006); however, glass microchannels are not ideal for the study of flow properties of blood at the microscopic level, primarily because of fabrication issues and physicochemical factors (Maeda 1996). First, glass-to-glass sealing is difficult because direct bonding needs extremely smooth and flat surfaces, and indirect bonding fills the channels with adhesives, sols, and metals. Second, the fabrication of microchannels in glass is limited in depth and width because glass is isotropically etched by hydrofluoric acid using a metal mask, which has a limited durability against the etchant. Moreover, the most suitable objective lenses for the confocal micro-PIV system have limited working distances (up to 0.5 mm), which requires special considerations in microchannel design. In addition to the fabrication limitations, several physical and biochemical factors contribute to the flow behavior of blood cells through microvessels. Glass microchannels differ from microvessels in several ways: the wall is not elastic, the flow channel is often straight and long, and the inner surface does not accommodate living endothelial cells. Hence, the results from classical *in vitro* experiments (Chien et al. 1984; Pries and Secomb 2003) that used glass microchannels need to be reexamined in the light of more sophisticated microchannels, such as polydimethysiloxane (PDMS) microchannels.

Because of these limitations with glass microchannels, it is important to develop a microfluidic device more closely representative of the *in vivo* microvascular environment using a reliable microfabrication technique compatible with the state-of-the-art flow measuring techniques, such as a confocal micro-PIV system. Using a soft lithography technique, it is possible to generate extremely precise, reproducible, and versatile rectangular microchannels. Although rectangular microchannels may not be the best models to simulate the geometry of microvessels *in vivo*, many aspects of blood flow behavior through this kind of microchannel are similar to those in living microvessels (Beebe et al. 2002; Shevkoplyas et al. 2003; Toner and Irimia 2005; Faivre et al. 2006). Furthermore, experiments with this kind of microchannel enable not only precise control of experimental parameters, but also accurate measurements. Thus, it is important to examine the applicability of the confocal micro-PIV system to measure both physiological saline (PS) and *in vitro* blood with a hematocrit (~20% Hct) close to that *in vivo* in PDMS microchannels. To our knowledge, no confocal micro-PIV measurements of PS and *in vitro* blood flow in a rectangular PDMS microchannel have been published. Thus, as a first step toward integrating a confocal micro-PIV with a PDMS microchannel, measurements were first performed in a simple, straight, rectangular microchannel.

In this study, we investigated the ability of our confocal micro-PIV system to measure the velocity profiles of physiological saline (PS) and *in vitro* blood at a normal Hct in a rectangular (300 μm wide, 45 μm deep) PDMS microchannel, fabricated by soft lithography. In particular, we compared the behavior of PS and *in vitro* blood flow (20% Hct) in a rectangular microchannel with a low aspect ratio. The results presented are also a verification as to the applicability of the confocal micro-PIV to obtain detailed measurements of blood flow with Hcts similar to those encountered in microvessels.

2 Materials and methods

2.1 Fabrication of the PDMS microchannel

PDMS polymers have many useful properties, including good optical transparency and biocompatibility, easily reversible sealing to glass, elasticity, replication of fine and complex geometries, permeability to gases, thermal stability, and low cost (Duffy et al. 1998; Chang et al. 2003; Mata et al. 2005; Kaji et al. 2006). Because of these properties, this material was suitable for studying several phenomena in the microcirculation by combining it with our confocal micro-PIV system.

The PDMS rectangular microchannel was developed using a soft lithographic technique. A detailed description of the fabrication process can be found elsewhere (Lima 2007). In brief, the photomask was first created using a pattern generator (Nihon Seiko, Japan) and then a solid master was fabricated on a glass substrate with an ultrathick photoresist (SU-8 50; Kayaku MicroChem, Japan). Metal wire posts were placed on the SU-8 mold master to create the connection channels to the input/output ports. The PDMS prepolymer was prepared by mixing a commercial prepolymer and catalyzer (Silpot 184; Dow Corning, USA) at a weight ratio of 10:1. After the mixture was degassed under vacuum, the PDMS was poured into the mold master and cured by baking for about 2h at 70°C. Both master and PDMS were cooled to room temperature and the PDMS was peeled from the master. The embedded metal wire posts were then pulled out of the PDMS. Finally, the PDMS was washed with ethanol and brought into contact with a clean glass, where a reversible seal formed spontaneously.

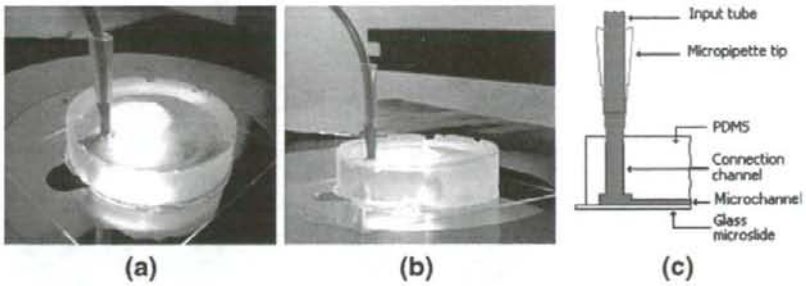

Fig. 1 PDMS microdevice with the input port (**a**) top view, (**b**) lateral view, (**c**) schematic drawing of the cross section

For this study, we found no need to make the PDMS hydrophilic by use of an oxygen plasma treatment.

The input/output ports were made by means of a 200-µl micropipette tip. This tip was inserted tightly into the connection channels where it exerted pressure on the PDMS and provided a liquid-proof seal. Top tubes (2.1 mm outer diameter, 1.1 mm inner diameter) were also fitted tightly into the micropipette to deliver the working fluids from the syringe pump (see Fig. 1). Due to the conical shape of the tip and low flow rates, we did not observe fluid leakage during our experiments. Thus, we found no need to use additional bounding adhesives, to avoid possible leakage from the microdevice.

To evaluate the performance of the confocal micro-PIV system by comparing experimental data with a theoretical model, it is important to both qualitatively and quantitatively verify the actual final geometry of the PDMS microchannel. Thus, the depth profile of the microchannel was carefully measured using a surface profiler (P-10; KLA Tencor, USA). Figure 2 shows the average depth from eight different measurements along the PDMS microchannel. The average depth was found to be 45 ± 1 µm. In addition, under a wide-field microscope, the average width was found to be 300 ± 2 µm. Thus, the measurement uncertainties for the depth and width of the microchannel were 2.2 and 0.7%, respectively. We also cut the PDMS microchannel transversely to measure the angle of the microchannel wall. We verified that the microchannel had a cross section that was nearly a perfect rectangular shape (300 µm wide, 45 µm deep). Figure 3 shows the cross section of the rectangular PDMS microchannel under an optical microscope.

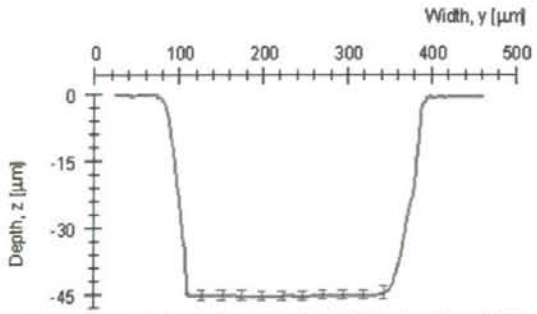

Fig. 2 Average depth of the rectangular PDMS microchannel. The measured values of the depth are expressed as the means ± standard deviation

2.2 Sample preparation: working fluids and blood samples

Two working fluids were used in this study: physiological saline (PS) and *in vitro* blood [PS containing ~20% (by volume) human red blood cells (RBCs)]. Fluids were seeded with 0.15% (*v/v*) 1-µm-diameter red fluorescent solid polymer microspheres (R0100; Duke Scientific, USA). For the *in vitro* blood, the fluorescent particles were first washed twice before seeding into the blood cell suspension.

Venous blood (~20 ml) was collected from a healthy, adult volunteer (aged 32years old) to make six samples with ~20% (by volume) RBCs suspended in PS. To prevent coagulation of the blood cells during the experiment, ethylenediaminetetraacetic acid (EDTA) was added to the glass tube. The RBCs were separated from bulk blood by centrifugation (3,000 rpm, 5 min) and aspiration of the plasma and buffy coat, and were then washed twice with PS. The washed RBCs were diluted with PS to make up the required RBC concentration by volume. The hematocrit of the RBC suspension was about ~20% (20% Hct) and the volume of each sample was 500 µl. Blood samples were stored at 4°C until the experiment was performed at room

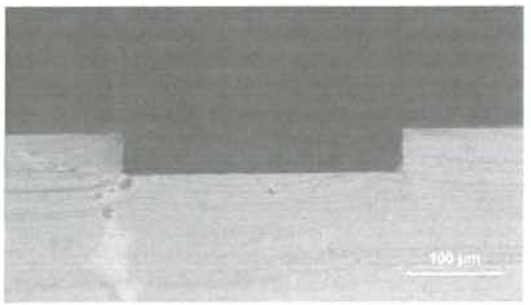

Fig. 3 Cross section of the PDMS microchannel

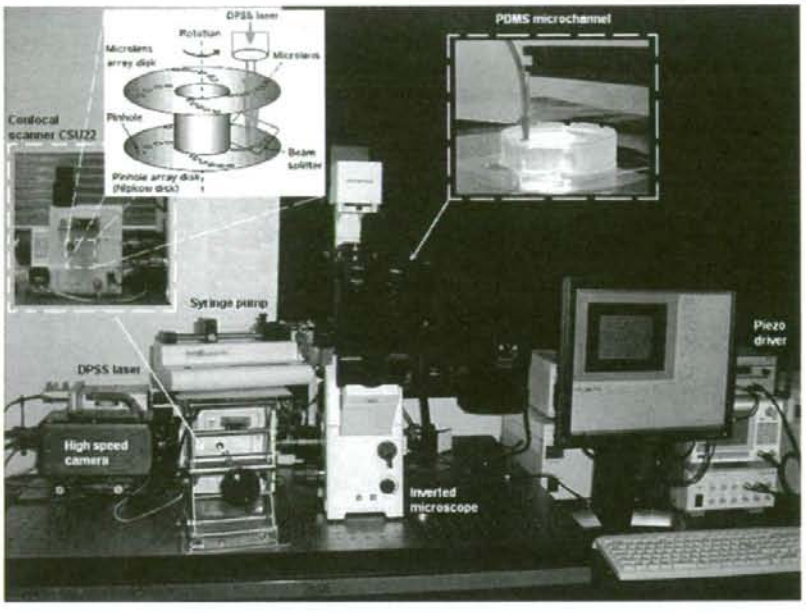

Fig. 4 Confocal micro-PIV experimental setup

temperature (25–27°C). All procedures in this experiment were carried out in compliance with the Ethics Committee on Clinical Investigation of Tohoku University.

2.3 Confocal micro-PIV experimental setup

The confocal micro-PIV system used in this study is shown in Fig. 4. A detailed description of the confocal system can be found elsewhere (Lima et al. 2006). In brief, the confocal system consisted of an inverted microscope (IX71; Olympus, Japan) combined with a confocal scanning unit (CSU22; Yokogawa, Japan), a diode-pumped solid-state (DPSS) laser (Laser Quantum, UK) with an excitation wavelength of 532 nm, and a high-speed camera (Phantom v7.1; Vision Research, USA). The laser beam was illuminated from the bottom of the microscope stage through a dry 20× objective lens with a numerical aperture (NA) of 0.75. The light emitted from the fluorescent tracers flowing within the microchannel passed through a color filter into the CSU22 scanning unit, where light was reflected by a dichromatic mirror onto a high-speed camera to record the PIV images.

The rectangular PDMS microchannel (300 μm wide, 45 μm deep, 10 mm long) was placed on the stage of an inverted microscope and using a syringe pump (KD Scientific, USA), a constant pressure-driven flow of 0.22 μl/min was maintained, corresponding to a Reynolds number (Re) of ~0.02 (based on the hydraulic diameter). A glass microsyringe (50 μl capacity) was used to obtain a flow rate as close as possible to a steady flow.

For the working fluids, PIV images were first captured with a resolution of 640 × 480 pixels, at a rate of 200 frames/s with an exposure time of 4995 μs and then recorded on a computer for evaluation using the Phantom camera control software (PH607). Using a dry 20×/0.75 NA objective lens, the estimated thickness of the measurement plane (optical slice thickness) was 4.97 μm. Moreover, using a high-speed

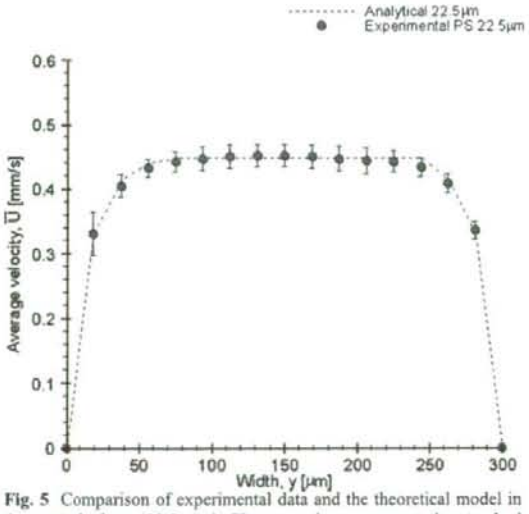

Fig. 5 Comparison of experimental data and the theoretical model in the central plane (22.5 μm). The *error bars* represent the standard deviation of six measurements using Student's *t* test with a 95% confidence interval

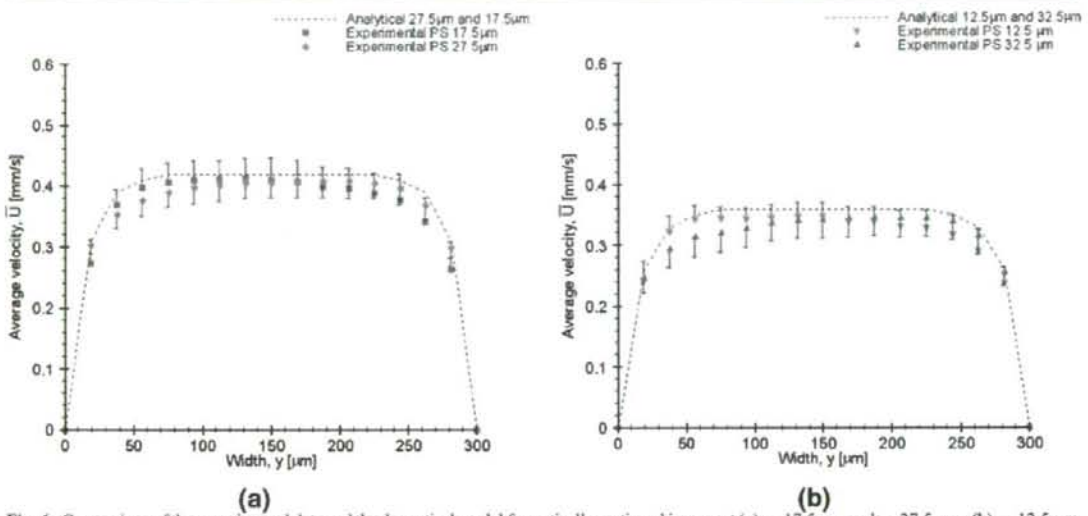

Fig. 6 Comparison of the experimental data and the theoretical model for optically sectioned images at (**a**) z=17.5 µm and z=27.5 µm; (**b**) z=12.5 µm and z=32.5 µm

objective lens actuator with submicron z-direction resolution it was possible to accurately capture optically sectioned images along the depth (z-axis) of the PDMS microchannel.

The PivView version 2.3 (PivTec, Germany) software (Willert et al. 1996; Raffel et al. 1998) was used to process the images by an iterative cross-correlation method (Willert et al. 1996; Raffel et al. 1998), while an advanced correlation technique (multi-grid interrogation) was used to improve the accuracy of the particle image displacement. The cross-correlation evaluation with grid refinement has been previously described (Willert et al. 1996; Raffel et al. 1998). In brief, the cross-correlation method is a statistical analysis that determines the average displacement by comparing the positions of the tracer particles within an interrogation area in two consecutive images. The cross-correlation function $R_{fg}(x, y)$ can be defined as (Raffel et al. 1998; Nguyen and Wereley 2002):

$$R_{fg}(x,y) = \sum_{i=1}^{p}\sum_{j=1}^{q} f(i,j)g(i+x,j+y), \quad (1)$$

where p and q are the dimensions (in pixels) of the interrogation area, and $f(i, j)$ and $g(i, j)$ represent the gray value distribution of the first and second image, respectively. The cross-correlation function correlates images of particles in two consecutive interrogation areas (particle image pair). The displacement of a particle image pair corresponds to the highest peak in the correlation plane. However, when small interrogation areas (usually less then 32 × 32 pixels) are used, random correlations can result in

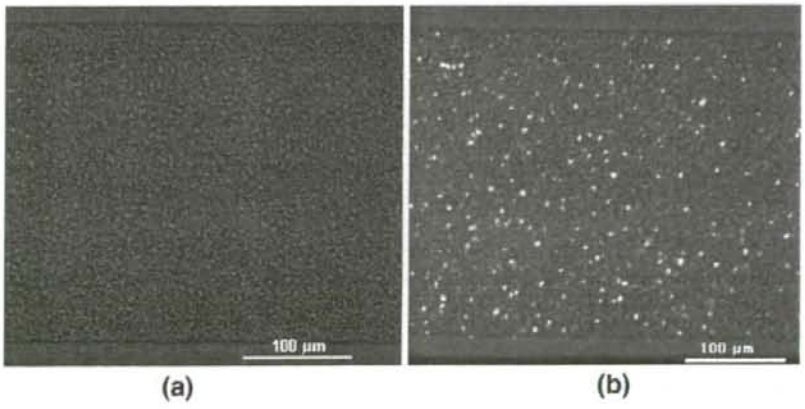

Fig. 7 (**a**) An image of *in vitro* blood (20% Hct) flow with halogen illumination. The RBCs are observed as dark grey rings. (**b**) Image of the same fluid in which both fluorescent particles and RBCs are visualised

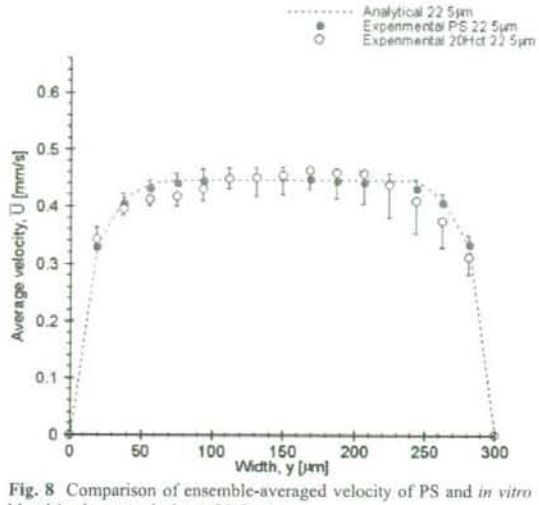

Fig. 8 Comparison of ensemble-averaged velocity of PS and *in vitro* blood in the central plane (22.5 μm)

noisy peaks and can generate an erroneous velocity vector (outlier). To reduce measurement uncertainty and to improve the signal-to-noise ratio, a multi-grid interrogation technique can be applied to the cross-correlation analysis (Raffel et al. 1998). The evaluation procedure of this advanced correlation technique is first based on a cross-correlation analysis at a relatively high correlation area (usually 32 × 32 pixels or more) to obtain an accurate estimate of the displacement and then the process is repeated at each pass by refining the interrogation area. By using this procedure, the displacement at a smaller interrogation area can be estimated with high accuracy, and consequently, high-resolution velocity vectors can be generated.

In our study, we used the iterative cross-correlation method, in which a multi-grid interrogation algorithm (grid refinement) was selected for evaluating the PIV image pairs. The initial interrogation area was 64 × 64 pixels whereas the final size was 24 × 32 pixel (50% overlap). Furthermore, the least squares Gauss fitting algorithm was used for detecting the peak on the correlation plane. Finally, the data were converted to the corresponding velocity fields using a magnification factor of 0.86 pixel/μm and pulse delay of 5 ms.

2.4 Ensemble averaged velocities

At steady flows, ensemble averaged velocities are known to improve the signal-to-noise ratio and consequently to generate more accurate velocity fields (Raffel et al. 1998; Meinhart et al. 2000). In this study, using the average velocity method, 100 instantaneous velocities measurements were ensemble-averaged to obtain the mean velocity field. This method first calculated the displacement field (peak detection) for each image pair and then the averaging operator was applied to all the instantaneous velocities measurements. The time-average mean velocity vector of the flow can be defined as

$$\vec{U} = \frac{\sum_{i=1}^{n} u_i}{n}, \tag{2}$$

where n is the number of valid instantaneous velocity measurements. In this study, we evaluated 100 images with time intervals of 5 ms.

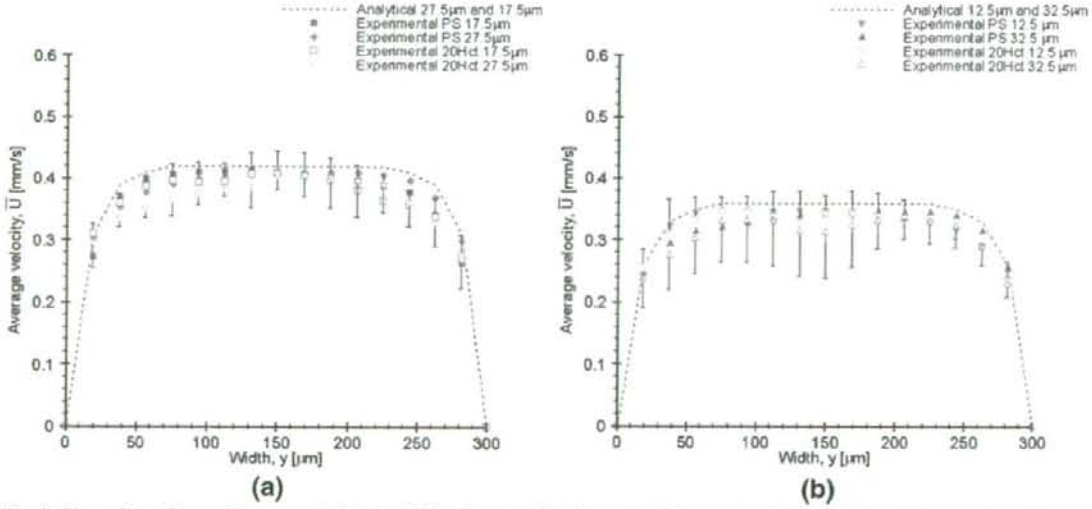

Fig. 9 Comparison of ensemble-averaged velocity of PS and *in vitro* blood at (**a**) z=17.5 μm and z=27.5 μm; (**b**) z=12.5 μm and z=32.5 μm

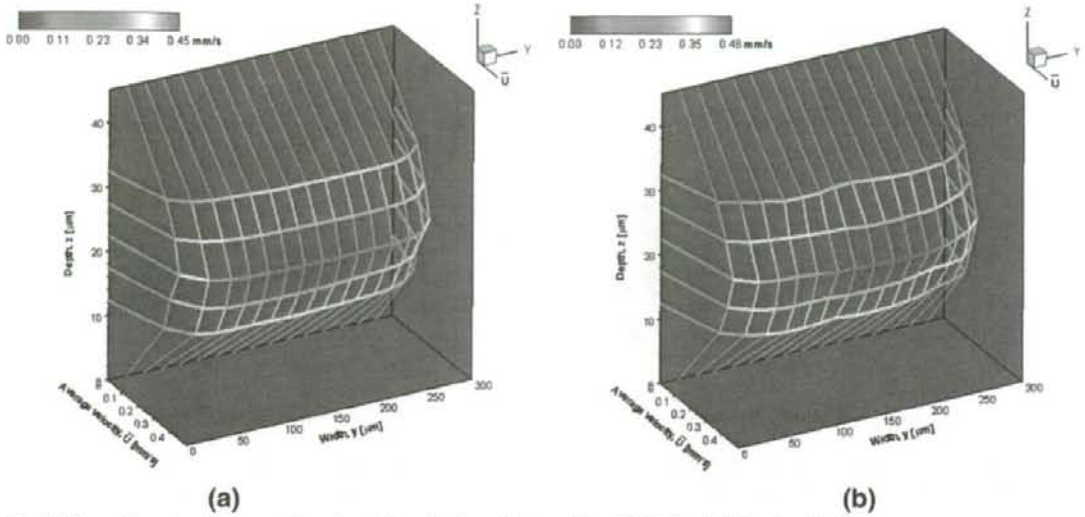

Fig. 10 Three-dimensional representation of optical sectioning velocity profiles of (a) PS and (b) *in vitro* blood

By calculating the u-component of the time-average mean velocity, it is possible to obtain the time-averaged velocity vector magnitude (U), which can be expressed as

$$U = \left|\vec{U}\right|. \tag{3}$$

The time-averaged velocity vector magnitude for six different samples ($\overline{U}$) was defined as

$$\overline{U} = \frac{1}{m \times n} \sum_{i=1}^{m} \sum_{i=1}^{n} U, \tag{4}$$

where m is the number of samples used and n is the number of grid points along the x-direction.

3 Results

3.1 Physiological saline

To evaluate the performance of the confocal micro-PIV system in measuring the velocity fields of the working fluids through the PDMS rectangular microchannel, the experimental results for PS were compared to a well-established analytical solution for steady flow through a long, straight, rigid rectangular microchannel, that of Poiseuille flow. The equation used to calculate the analytical velocity profile of

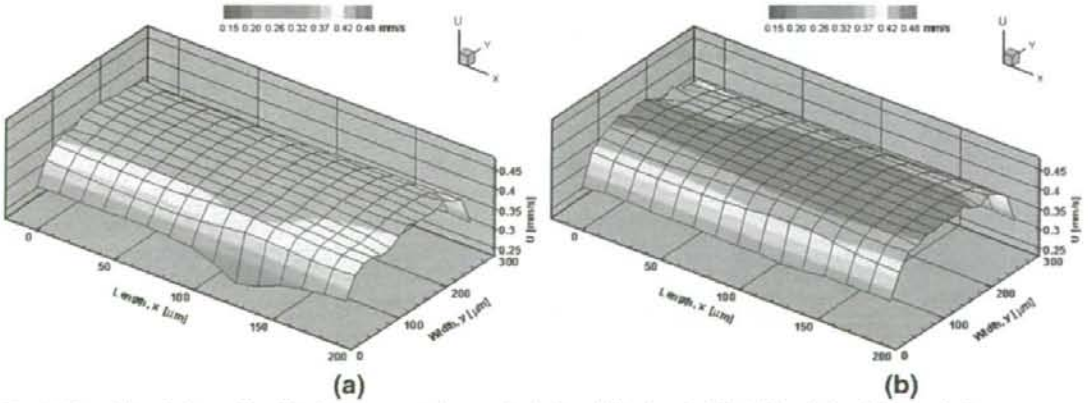

Fig. 11 Ensemble velocity profiles (U) of two representative samples in the middle plane for PS. (a) Sample 1 and (b) sample 2